Dalton Transactions

PAPER

View Article Online
View Journal | View Issue

Cite this: *Dalton Trans.*, 2018, **47**, 15082

SSZ-70 borosilicate delamination without sonication: effect of framework topology on olefin epoxidation catalysis†

Alexander Okrut, [a] Martina Aigner, [a] Christian Schöttle, [a] Nicolás A. Grosso-Giordano, [a] Son-Jong Hwang, [b] Xiaoying Ouyang,*[c] Stacey Zones*[c] and Alexander Katz *[a]

We report a scalable delamination procedure for a SSZ-70-framework layered-zeolite precursor, which for the first time does not involve either sonication or long-chain surfactants. Our approach instead relies on the mild heating of layered zeolite precursor B-SSZ-70(P) in an aqueous solution containing $Zn(NO_3)_2$ and tetrabutylammonium fluoride. Powder X-ray diffraction data are consistent with a loss of long-range order along the *z*-direction, while ^{29}Si MAS NMR spectroscopy demonstrates preservation of the zeolite framework crystallinity during delamination. The resulting delaminated material, DZ-2, possesses 1.4-fold higher external surface area relative to the nondelaminated three-dimensional zeolite B-SSZ-70, based on N_2 physisorption data at 77 K. DZ-2 was functionalized with cationic Ti heteroatoms to synthesize Ti-DZ-2 *via* exchange with framework B. Ti-DZ-2 contains isolated titanium centers in its crystalline framework, as shown by UV-Vis spectroscopy. The generality of the synthetic delamination approach and catalyst synthesis is demonstrated with the synthesis of delaminated material DZ-3, which is derived from layered zeolite precursor ERB-1(P) with MWW framework topology. Upon catalytic testing for the epoxidation of 1-octene with ethylbenzene hydroperoxide as oxidant, under harsh tail-end conditions that deactivate amorphous Ti-silica-based catalysts, Ti-DZ-2 exhibits the highest per-Ti-site activity, selectivity, and stability for 1-octene epoxidation of all catalysts investigated. This testing includes the prior benchmark delaminated zeolite catalyst in this area, Ti-UCB-4, which possesses similar external surface area to Ti-DZ-2 but requires sonication and long-chain surfactants for its synthesis. The synthesis of DZ-2 is the first example of an economical delamination of layered zeolite precursor SSZ-70(P) and opens up new doors to the development of delaminated zeolites as commercial catalysts.

Received 25th July 2018,
Accepted 3rd October 2018

DOI: 10.1039/c8dt03044h

rsc.li/dalton

Introduction

The synthesis of zeolites with high external surface area is motivated by the need to overcome diffusional limitations inherent to microporous frameworks, enabling the accessibility of reactants to catalytic active sites on the external surface, while retaining structural features of the zeolite in two dimensions.[1–9] Delamination of layered zeolite precursors strives to be one such practical synthetic method, though it is limited to materials that proceed in their synthesis through a layered zeolite precursor. Recent progress in zeolite delamination has focused on developing techniques for exfoliation that avoid damage to the zeolite framework, such as possible amorphization during high-pH treatments.[10–14] Within this area, a goal has been to eliminate steps involving costly surfactant swelling and sonication, in order to facilitate scalability of delaminated-material synthesis. Recently, we demonstrated how this can be accomplished in the delamination of layered zeolite precursor ERB-1(P) – a zeolite consisting of a neutral piperidine rather than cationic quaternary ammonium organic structure directing agent (SDA) – *via* Zn treatment followed by calcination and ZnO removal, to synthesize delaminated material DZ-1.[13]

However, the sonication-free synthesis of delaminated zeolites *via* Zn treatment has until now been impossible to perform with the structurally related SSZ-70, which, like ERB-1, consists of stacked layers consisting of hemispherical cups,[15]

[a]*Department of Chemical and Biomolecular Engineering, University of California at Berkeley, Berkeley, California 94720, USA. E-mail: askatz@berkeley.edu*
[b]*Division of Chemistry and Chemical Engineering, California Institute of Technology, Pasadena, California 91125, USA*
[c]*Chevron Energy Technology Company, Richmond, California 94804, USA. E-mail: sizo@chevron.com*

†Electronic supplementary information (ESI) available. See DOI: 10.1039/c8dt03044h

but relies instead on a cationic SDA (*e.g.*, diisobutylimidazolium hydroxide) for its synthesis.[13] We previously demonstrated that it was the cationic nature of the SDA that prevented SSZ-70 layered zeolite precursor delamination under the conditions used for synthesis of DZ-1.[13] The lack of an available sonication-free delamination method for SSZ-70 precursors significantly limits the practical application of delaminated zeolites prepared from this layered precursor, despite its superior catalytic performance. The superior performance of SSZ-70 is described in recent studies, where the delaminated form of Al-SSZ-70, UCB-3, exhibits high activity as a Brønsted acid aromatic alkylation catalyst while retaining the same shape selectivity as 3D zeolites such as Al-MCM-22.[16] More recently, delamination of B-SSZ-70 to UCB-4 facilitates the incorporation of a variety of metal heteroatoms into the SSZ-70 delaminated-zeolite framework,[13] including Ti,[17,18] which has exhibited highly robust and active olefin epoxidation catalysis with organic hydroperoxide as oxidant. In particular, Ti incorporated in UCB-4 (delaminated and deboronated SSZ-70), Ti-UCB-4, has emerged as a robust (*i.e.* less prone to deactivation) solid catalyst for terminal-olefin epoxidation, superior in performance to current industrial benchmark catalysts.[19,20] This is shown by lower rates of deactivation of Ti-UCB-4 compared to conventional catalysts based on an amorphous silica support, which represent models of industrial catalysts for propylene oxide synthesis using organic hydroperoxide as oxidant, under the highly deactivating environments found at the tail-end of industrial propylene-epoxidation flow reactors.[19,20] Incorporating Ti into delaminated-zeolite frameworks has been shown to increase their catalytic epoxidation activity compared to their nondelaminated three-dimensional counterparts, as has been demonstrated for MCM-22,[21–24] TS-2,[25] and HUS-7.[26] This makes Ti incorporated within delaminated zeolite frameworks an attractive candidate for a new generation of crystalline olefin epoxidation catalysts, but challenges associated with the cost and scalability of the delamination procedure must be overcome.

With these thoughts in mind, this manuscript describes a novel, scalable, sonication-free approach for the delamination of B-SSZ-70(P), which obviates the need for swelling with long-chain surfactants, two components that currently limit the cost and scalability of zeolite delamination. The resulting delaminated zeolites are acid-washed to yield delaminated zeolite DZ-2, which contains exposed vacancy defects that are templated by framework boron, which is removed during acid washing. These so-generated silanol nests can be re-occupied by Ti *via* cation grafting to synthesize Ti-DZ-2. We compare this latter catalyst with previously reported Ti-UCB-4, which is synthesized *via* a conventional delamination route, which requires costly and cumbersome surfactant swelling and sonication steps, as well as with delaminated zeolite Ti-DZ-3, which is synthesized from layered zeolite precursor ERB-1 (borosilicate MWW) *via* a similar procedure to that used in the synthesis of Ti-DZ-2. The latter demonstrates the generalization of our delamination approach to other layered zeolite precursors and allows us to cleanly assess the role of framework topology on Lewis-acid catalysis here, by keeping the same delamination synthetic approach across differing framework topologies. The catalysis system used is the epoxidation of 1-octene with ethylbenzene hydroperoxide, a well-known Lewis-acid-catalyzed probe reaction, where emphasis is placed on stability of performance under harsh tail-end conditions of the epoxidation reactor, as we have performed previously, in order to differentiate the stability of various catalysts under what are known to be deactivating conditions.[19,20] We note that a rigorous comparison of different delaminated zeolite topologies has thus far not been possible, because our previous attempts to compare SSZ-70 and MWW frameworks of Ti-delaminated-zeolite catalysts were obscured by changes in the delamination method.[13,17] We anticipate that approaches such as this one, where layered zeolite precursors from varying topologies can be delaminated under identical conditions, will facilitate catalytic comparisons of other two-dimensional zeolites.[21,27]

Our approach for the delamination of B-SSZ-70(P) is shown in Fig. 1a. It leverages on previously described approaches for delamination of ERB-1(P) (B-MWW layered zeolite precursor material), using an aqueous solution of $Zn(NO_3)_2$.[13] A crucial advance here has been the delamination of a layered zeolite precursor without either long-chain surfactants or sonication, even for a precursor comprising a quaternary ammonium SDA, by a combination of a fluoride mineralizing agent, consisting of tetrabutylammonium fluoride (TBAF), in conjunction with $Zn(NO_3)_2$. This approach is exemplified for both SSZ-70 and MWW framework topologies with the delamination of B-SSZ-70(P) and ERB-1(P), as shown in Fig. 1a and b, respectively. These two precursors have different structures,[15] though they share some similarities such as a lamellar precursor structure and external-surface cups arising from 12-membered ring units within the framework. Within the context of previous research in delaminated zeolite synthesis, TBAF has been used in conjunction with tetrabutylammonium chloride (TBACl), and long-chain surfactants for swelling B-SSZ-70(P), as well as sonication to affect delamination of B-SSZ-70(P) (see Fig. 1c).[28,29] However, as mentioned above, this delamination was impossible to accomplish with Zn treatment alone.[13]

Experimental

Materials

All reagents in this manuscript were reagent-grade quality and were used as received unless otherwise noted. Syntheses of materials B-SSZ-70, ERB-1, and UCB-4 were performed as previously described.[13,28]

Synthesis of DZ-2 and DZ-3 precursor

0.5 g of layered zeolite precursor (consisting of B-SSZ-70(P) in the case of DZ-2 synthesis and ERB-1(P) in the case of DZ-3 synthesis), 0.85 g of tetrabutylammonium fluoride and 2.0 g of zinc nitrate hexahydrate was added to 20 mL of deionized water. The reaction mixture was vigorously stirred at 135 °C for

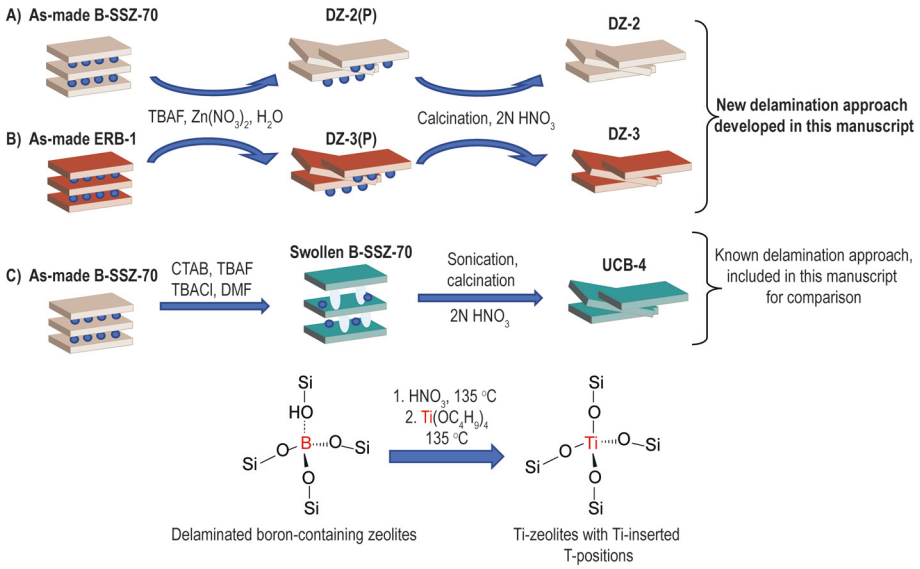

Fig. 1 Schematic diagram of the new surfactant-free approach for zeolite delamination (A and B) and the conventional surfactant-mediated method for zeolite delamination (C). Both conventional and new approaches lead to exfoliation of layered zeolite precursors into delaminated zeolites DZ-2, DZ-3, and UCB-4, consisting of a high density of silanol nests as a result of deboronation.

16 h. The solid product was collected on a filter, washed thoroughly with deionized water followed by acetone, and then air dried.

Calcination of the DZ-2 and DZ-3 precursor

The DZ-2 and DZ-3 precursors were calcined at 550 °C in air for 5 h. The ramp rate was 1 °C min^{-1}.

Synthesis of DZ-2 and DZ-3

0.5 g of calcined precursor was added to 50 mL of 2 N HNO_3. The slurry was vigorously stirred at 135 °C overnight. The solid product was collected on a filter, washed thoroughly with deionized water followed by acetone, and then air dried.

Synthesis of Ti-DZ-2, Ti-DZ-3, Ti-UCB-4, Ti-ERB-1, and Ti-SSZ-70

0.5 g of zeolite was dried in a 15.0 mL high-pressure flask at 120 °C for at least 3 hours. Under a stream of argon, 5.0 mL of anhydrous 1-butanol and 0.5 mL of titanium(IV)-*n*-butoxide were added. The mixture was stirred at 135 °C for 1 hour. After cooling to room temperature, the suspension was filtered and washed with 1-butanol. After drying at 120 °C, the white powdered product was crushed with a pestle and calcined at 550 °C for 10 hours.

Characterization methods

Powder X-ray diffraction (PXRD) patterns were collected on a Bruker GADDS D-8 diffractometer using Cu Kα radiation. Data were collected in the 2θ range from 3° to 30° with a step size of 0.02° and a dwell time of 2 s. Nitrogen physisorption isotherms were measured on a Micromeritics ASAP2020 instrument at 77 K. Prior to measurement, samples were evacuated at 350 °C for 4 h. Acridine (Sigma Aldrich, 97%) was recrystallized two times in ethanol and used to prepare a 500 μmol acridine per g *n*-octane stock solution. 2 mL of the acridine stock solution was added to approximately 3.00 mg zeolite for titration of external acid sites at room temperature, corresponding to a three-fold excess of estimated acid sites present in the zeolite sample. The titrated solution was collected after 1 h and passed through a 0.2 μm syringe filter. The difference of UV-Vis absorbance of the stock solution and titrated solution was recorded using a Varian Cary 400 UV-Vis spectrometer and was found to give accurate external acid-site densities, within a spread of 5% after three replicate experiments. High-angle annular dark-field scanning transmission electron microscopy (HAADF-STEM) was conducted with a FEI Tecnai F20 operated at 200 keV. Samples suitable for HAADF-STEM were prepared on amorphous Lacey-carbon films deposited on copper grids (Ted Pella, Inc.).

Olefin epoxidation

Zeolite catalysts were pelletized to a particle size of 180 μm–250 μm. 25 mg of calcined catalyst was packed into a stainless-steel reactor (l = 41 mm, ∅ = 6 mm) between layers of glass wool. Layers of glass beads before and after the catalyst layer were used to stabilize the catalyst bed in the middle of the reactor and to enable thorough mixing of the reaction solution. The reaction solution consisted of 1029.0 mmol (115.5 g) of 1-octene, 32.1 mmol (4.4 g) of EBHP, 62.4 mmol (8.7 g) of ethylbenzene, 188.4 mmol (24.2 g) of 1,2-epoxyoctane, 2.7 mmol (1.5 g) of acetophenone, 186.6 mmol (22.8 g) of 1-phenylethanol and 11.9 mmol (1.5 g) of *n*-nonane as an internal standard. The packed reactor was heated under vacuum at 140 °C for at least 4 hours. After cooling to room temperature, the reactor was flushed with 1-octene and connected to a syringe that contained the reaction solution. The required flow rate was controlled using a syringe pump. The

reactor was submerged in an oil-bath, which was held at a temperature of 110 °C. Samples were collected for a duration of 1 hour, over different periods of time on stream. In order to allow the system to equilibrate, sample collection started at least 2 h after the experiments were started. Reactor outlet samples were analyzed by gas chromatography using *n*-nonane as an internal standard. Liquid samples were analyzed for reactants and products by gas chromatography (Agilent 6890, HP-1 methylsilicone capillary column), from which reaction rates and selectivities were calculated.

Results and discussion

Synthesis and characterization of delaminated zeolites Ti-DZ-2 and Ti-DZ-3

Powder X-ray diffraction (PXRD) was used to investigate crystallinity and structural integrity of the delaminated zeolite samples before and after delamination. The top graph in Fig. 2 shows the PXRD pattern of calcined materials consisting of delaminated zeolite DZ-2, in comparison with conventional delaminated B-SSZ-70 zeolite UCB-4, which requires sonication for its delamination, and three-dimensional zeolite B-SSZ-70, the calcined B-SSZ-70 layered zeolite precursor. The bottom graph in Fig. 2 shows the powder diffraction pattern of calcined material DZ-3 in comparison with its corresponding three-dimensional zeolite, ERB-1. The peaks of DZ-2 and UCB-4 at 7.2°, 7.9°, and 9.9° 2θ match B-SSZ-70 and the characteristic peak positions of DZ-3 at 7.2°, 8.1°, and 10.1° 2θ match those of ERB-1. This is consistent with all samples retaining crystallinity within a given zeolite layer, and delamination not destroying (*i.e.* making amorphous) the zeolite framework for DZ-2, DZ-3, and, as reported previously,[28] UCB-4. We therefore conclude that the crystalline structure within the two-dimensional zeolite-layer building blocks consisting of DZ-2, UCB-4, and DZ-3 is retained, as it is for parent materials B-SSZ-70 and ERB-1. Peaks in the PXRD patterns of Fig. 2 that correspond to ordering along the *z*-direction perpendicular to the zeolite layers are [011] and [012] and are located at 7.9° ([011]) and 9.9° ([012]) 2θ for DZ-2 and UCB-4, and 8.1° ([011]) and 10.1° ([012]) 2θ for DZ-3 and ERB-1. All of these peaks show severe broadening and intensity loss after delamination in materials DZ-2, UCB-4, and DZ-3, when compared to calcined three-dimensional materials B-SSZ-70 and ERB-1. Such broadening and intensity loss are indicative of loss of long-range order along the crystallographic *z*-axis, perpendicular to zeolite layers, consistent with delamination in DZ-2, UCB-4, and DZ-3.

N_2-Physisorption data for all investigated frameworks are shown in Fig. 3. Table 1 summarizes physicochemical pro-

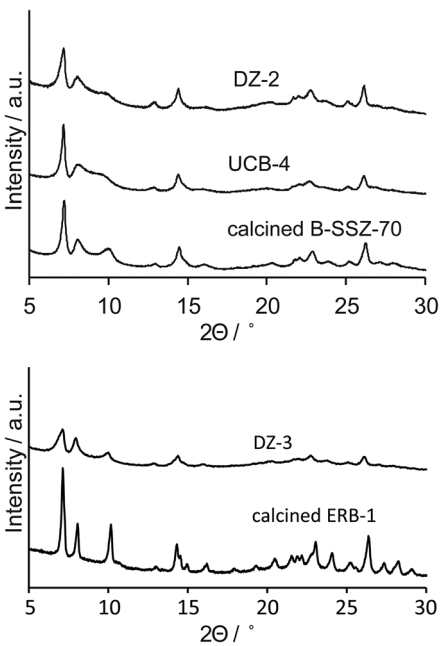

Fig. 2 Powder XRD pattern of calcined materials consisting of B-SSZ-70, UCB-4, DZ-2, ERB-1, and DZ-3.

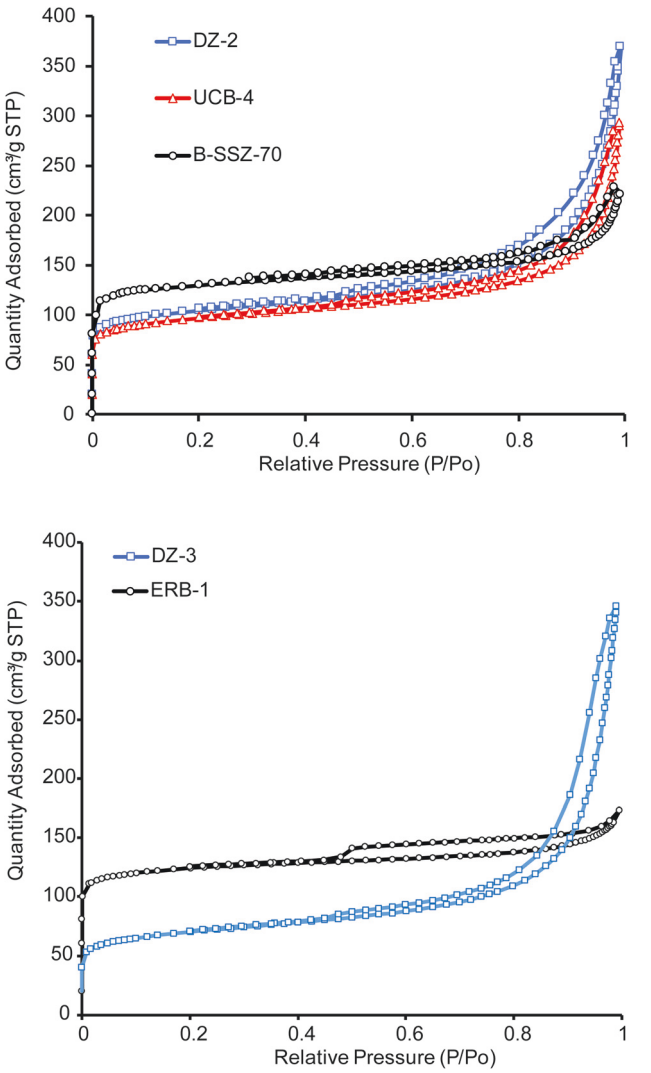

Fig. 3 N_2 physisorption plots of calcined materials consisting of DZ-2, UCB-4, DZ-3, B-SSZ-70, and ERB-1.

Table 1 Physicochemical properties of DZ-2, UCB-4, DZ-3, B-SSZ-70, and ERB-1 materials

Sample	S_{ext}	S_{tot}	V_{micro}	V_{total}
DZ-2	110	385	0.11	0.55
UCB-4	107	357	0.10	0.44
B-SSZ-70	79	494	0.17	0.34
DZ-3	94	254	0.07	0.51
ERB-1	50	471	0.17	0.25

perties for all calcined materials, which show characteristic type I/IV-mixed isotherms, indicating presence of both micro- and mesopores. Delaminated zeolites DZ-2, UCB-4, and DZ-3 show less N_2 uptake in the micropore region between $P/P_0 = 0$ and $P/P_0 = 0.1$, when compared to the corresponding 3D zeolites, B-SSZ-70 and ERB-1. This is consistent with the loss of micropores upon delamination, which would otherwise be located between zeolitic layers in the three-dimensional zeolites B-SSZ-70 and ERB-1. The increase of external surface area during delamination is clear when comparing the slope of the isotherm region between $P/P_0 = 0.2$ and $P/P_0 = 0.7$ in Fig. 3. Isotherms for DZ-2, UCB-4, and DZ-3 exhibit a steeper slope than for calcined three-dimensional zeolites B-SSZ-70 and ERB-1, indicating higher external surface area for the delaminated materials, and this is quantified *via* the t-plot method in Table 1. The mesopore region between $P/P_0 = 0.7$ and $P/P_0 = 1$ shows a higher N_2 uptake for DZ-2, UCB-4, and DZ-3 compared to the corresponding three-dimensional materials consisting of B-SSZ-70 and ERB-1. This can be explained by the synthesis of larger mesopores between zeolitic sheets as a result of delamination. The absence of such mesopores in calcined three-dimensional B-SSZ-70 and ERB-1 materials leads to lower N_2 uptake in this region. Altogether, physisorption data are consistent with loss of microporosity and addition of mesoporosity as a result of delamination, during synthesis of DZ-2, DZ-3, and UCB-4. Though the increases in external surface area are modest (factors of 1.3 and 1.4) compared to previously reported materials, such as ITQ-2 and MCM-56,[9,22] we demonstrate below that materials DZ-2 and DZ-3 have distinct catalytic advantages over their nondelaminated comparative counterparts.

Characterization by ^{29}Si MAS NMR and ^{29}Si CP/MAS NMR spectroscopies was performed for the parent layered zeolite precursor B-SSZ-70(P), delaminated material DZ-2, and conventionally delaminated Ti-UCB-4. These data are shown in Fig. 4 and Table 2. All materials consist of Q^4 and Q^3 silicon sites in the region of −93 to −123 ppm, with no evidence of Q^2 sites, which would otherwise have been apparent in the region immediately downfield of −90 ppm.[30] The Q^3 silicon resonance at −94 ppm present in as-made samples of B-SSZ-70 and DZ-2(P) disappears upon calcination at 550 °C, indicating that the contributing Q^3 silicon atoms condense to form Si–O–Si bonds during calcination. The lack of Q^2 resonances is consistent with a lack of amorphization of the silicate framework in all delaminated materials. We therefore infer that all methods employed here for affecting zeolite delamination and metal heteroatom insertion (including the new approach

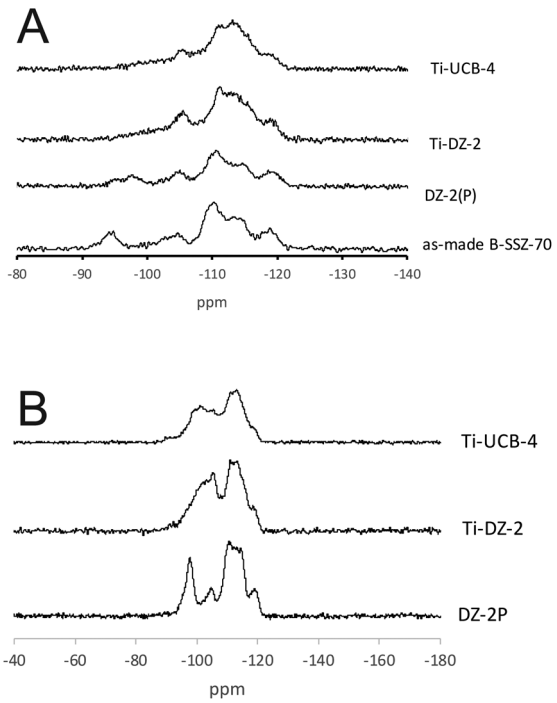

Fig. 4 (A) MAS ^{29}Si NMR spectra, and (B) CP MAS ^{29}Si NMR spectra of selected materials. NMR spectra were collected using a Bruker DSX-500 MHz spectometer and a Bruker 4 mm MAS probe. Spinning rate was 8 kHz.

Table 2 Q^3/Q^4 ratio derived from ^{29}Si NMR data of selected samples

Sample	Q^3/Q^4 ratio
Calcined Ti-DZ-2	0.11
As-made DZ-2	0.20
Calcined Ti-UCB-4	0.16
Deboronated[a] UCB-4	0.24
As-made B-SSZ-70	0.19

[a] Calcined prior to deboronation.

based on Zn treatment) are gentle on the zeolite framework and do not cause hydrolytic breakdown/amorphization of the framework. This is consistent with the retention of crystallinity following delamination in the PXRD data of Fig. 2 discussed above. This conclusion is similar to ones made in development of previous Zn-based mild delamination strategies for ERB-1 (P), which also did not cause zeolite amorphization.[13]

We calculated Q^3/Q^4 ratios for as-made and calcined materials in Table 2 to confirm the preservation of the crystalline framework during delamination as well as to detect the formation of silanol nests after acid-washing the delaminated zeolites. The similar Q^3/Q^4 ratios for as-made B-SSZ-70(P) and as-made DZ-2 in Table 2 are consistent with the gentle nature of delamination, which retains the crystalline framework during DZ-2 synthesis and does not synthesize amorphous regions from the crystalline zeolitic framework. We observed a nearly 50% decrease in the Q^3/Q^4 ratio in Ti-DZ-2 after its calcination. This is attributed to external silanol condensation, presumably

between delaminated-zeolite layers, during high temperature treatment. In comparison, calcined Ti-UCB-4 consists of a slightly larger Q^3/Q^4 ratio in Table 2, relative to Ti-DZ-2.

^{11}B NMR spectroscopy of as-made B-SSZ-70 and DZ-2 demonstrate loss of ~50% of the framework boron during delamination *via* Zn treatment (see Fig. S2†). Thus, we infer that a high proportion of the sites in as-made B-SSZ-70 that were originally occupied by boron now consist of framework vacancies (silanol nests) after delamination *via* Zn treatment, even prior to acid treatment, which is applied as a subsequent step to affect Zn removal and to remove all of the remaining B in DZ-2. Closely associated silanols within these framework vacancies, which serve as grafting centers for Ti precursors, are expected to condense during calcination of DZ-2,[18] but will be repopulated during the final acid wash.[31] The absence of residual B within calcined and acid-washed DZ-2 (as well as UCB-4) is evident in the lack of signal intensity in the ^{11}B NMR spectrum. We thus conclude that both of these materials (*i.e.* DZ-2 and UCB-4) have been completely deboronated.

Successful incorporation of Ti framework heteroatoms into delaminated zeolites is confirmed for all materials by UV-Vis spectroscopy, as shown in Fig. 5. All spectra exhibit a maximum in absorption intensity (Kubelka Munk units) in the range of 209 nm–229 nm, bands that are assigned to isolated Ti sites in framework locations.[32] All spectra show a slight shoulder around 260 nm, indicating that a slight fraction of titanium sites in non-framework positions (*i.e.* those grafted onto external-surface isolated silanols).

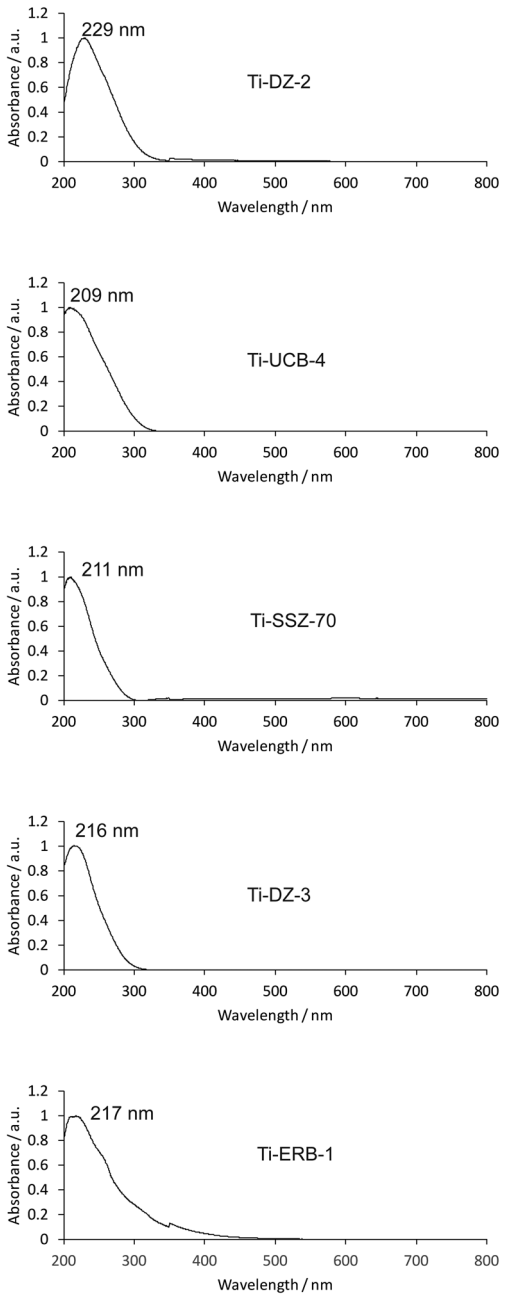

Fig. 5 UV-Vis spectra of calcined materials consisting of Ti-DZ-2, Ti-UCB-4, Ti-DZ-3, Ti-SSZ-70, and Ti-ERB-1.

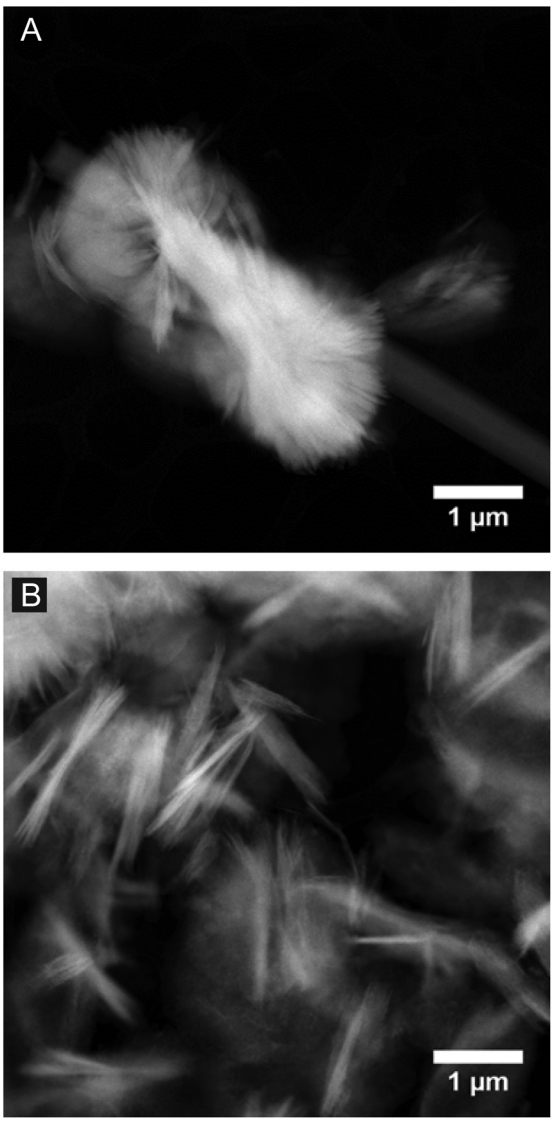

Fig. 6 HAADF-STEM images of B-SSZ-70 (A) and DZ-2 (B).

HAADF-STEM (high-angle annular dark-field scanning transmission electron microscopy) images of the three-dimensional B-SSZ-70 and the delaminated DZ-2 are shown in Fig. 6 and Fig. S3 (ESI†). While data in Fig. 6a and Fig. S3a† shows calcined B-SSZ-70 to consists of large bundles of zeolitic layer in bulky clumps on the micron length scale, delaminated DZ-2 in Fig. 6b and Fig. S3b† exhibits a less dense morphology, consisting of thinner stacks and even isolated layers of the same zeolitic sheets. No amorphous phases were observed in both samples. Altogether, these data confirm the delamination of B-SSZ-70 to DZ-2.

Olefin epoxidation catalysis

In order to assess the effect of the delamination method on Lewis acidity and catalysis by grafted Ti sites, we performed epoxidation of the terminal olefin 1-octene with ethylbenzene hydroperoxide (EBHP) as oxidant, as a relevant probe reaction, for delaminated-material catalysts consisting of Ti-DZ-2, Ti-UCB-4, and Ti-DZ-3, as well as the corresponding nondelaminated catalysts Ti-SSZ-70 and Ti-ERB-1. This reaction was performed in a flow reactor under tail-end conditions (*i.e.*, the feed to the reactor consists of products and by-products, simulating 80% EBHP conversion at 99.9% selectivity to 1,2-epoxyoctane), as used previously for the characterization of grafted Ti siliceous catalysts.[19,20] The long-term (1 week) catalytic stability and selectivity data for catalysts Ti-DZ-2, Ti-UCB-4, and Ti-DZ-3 are compared in Fig. 7, which shows time-on-stream data for all three materials. The EBHP conversion when using catalyst Ti-DZ-2, Ti-UCB-4, and Ti-DZ-3 remains constant after reaching a steady-state after around 70 h time on stream, and the steady-state selectivity (*i.e.* fraction of converted EBHP that goes into synthesis of 1,2-epoxyoctane) for these catalysts is 81%, 73%, and 73%, respectively. The performance of all materials is stable with time on stream, with respect to lack of long-term deactivation. The steady-state selectivity of Ti-DZ-2 is observed to be higher than for Ti-UCB-4. Since both Ti-DZ-2 and Ti-UCB-4 are derived from the same B-SSZ-70 precursor material, we exclude effects of Ti-site location within the framework as causing the difference in selectivity.[19,20] Similar trends are observed for 1-octene epoxidation with EBHP when

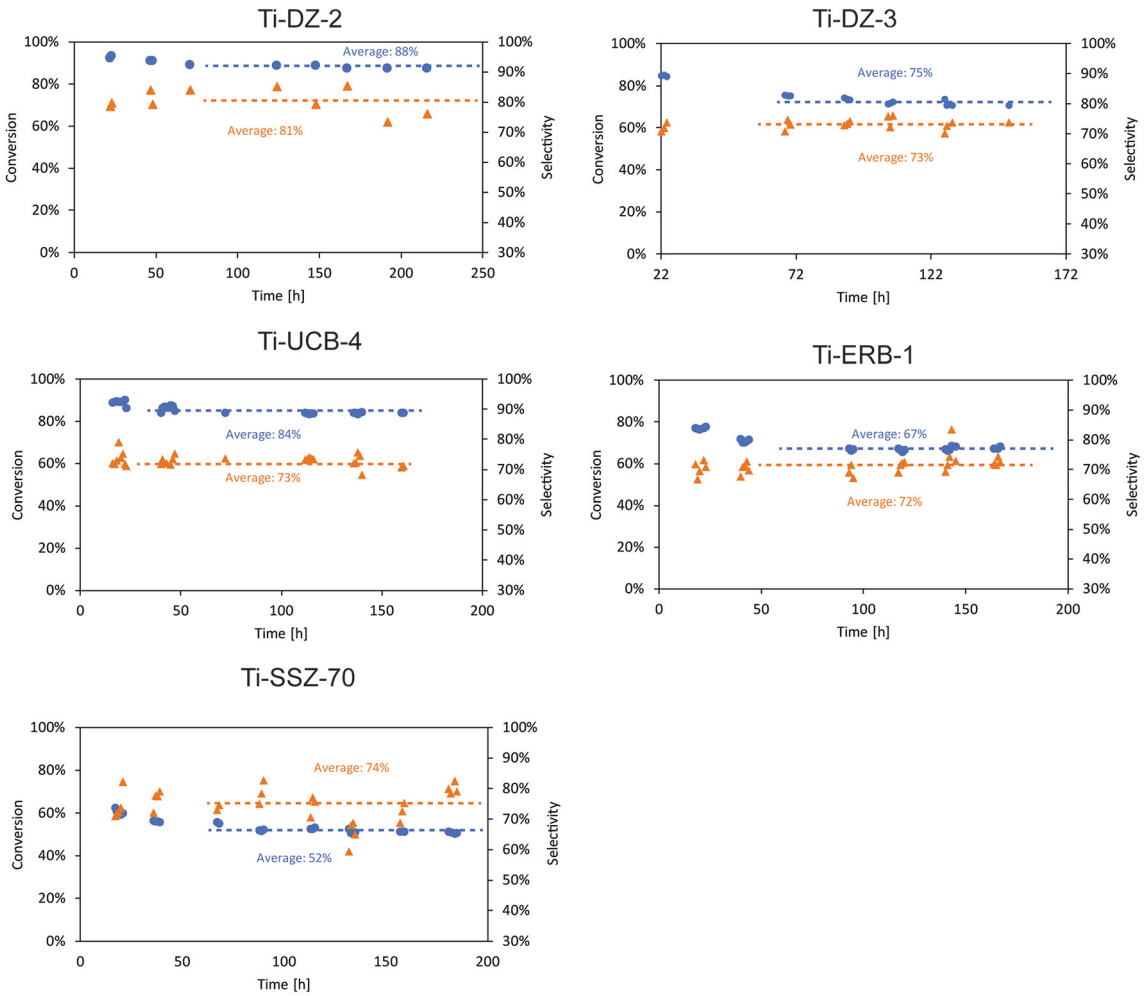

Fig. 7 1-Octene epoxidation performance in a flow reactor of Ti-DZ-2, Ti-UCB-4, Ti-DZ-3, Ti-SSZ-70, and Ti-ERB-1. Blue symbol (●) depicts EBHP conversion and orange symbol (▲) depicts selectivity of EBHP for 1-octene.

Table 3 Characteristics of Ti-catalysts for 1-octene epoxidation with EBHP as oxidant. Rate constants k and k' represent averages over the entire flow-reactor run, as they were calculated based on all kinetic data

Sample	Ti-Concentration [μmol g^{-1}]	External surface area [m^2 g^{-1}]	UV-Vis peak maximum [nm]	Reaction rate constant k', mass-based [mL h^{-1} g^{-1}]	Reaction rate constant k, Ti-based [10^3 mL h^{-1} g^{-1}]	Selectivity [%]
Ti-DZ-2	73	110	229	94	26.6	81
Ti-UCB-4	86	101	209	72	17.8	73
Ti-DZ-3	86	94	216	64	15.7	73
Ti-SSZ-70	46	79	211	29	13.3	74
Ti-ERB-1	29	50	217	21	15.7	71

using the nondelaminated 3-D zeolites Ti-SSZ-70 and Ti-ERB-1 as control catalysts, where EBHP conversion remains nearly constant throughout 70 h–160 h time on stream, with 74% (Ti-SSZ-70) and 72% (Ti-ERB-1) selectivity, similar to the selectivities observed for the corresponding delaminated-zeolite catalysts. This stability and lack of deactivation differentiates all three delaminated zeolites from catalysts based on an amorphous silica support, which we previously showed to deactivate under similar conditions (resulting in a decrease of the EBHP conversion with increasing time on stream).[20]

Table 3 shows calculated pseudo-first-order rate constants on a catalyst mass and Ti-site basis (assuming an ideal plug-flow reactor). Ti-DZ-2 is the most active catalyst on both a catalyst mass and Ti-site basis, with a mass-based rate constant k of 94 mL h^{-1} g^{-1}, higher than Ti-UCB-4 and Ti-DZ-3, with corresponding rate constants k of 72 mL h^{-1} g^{-1} and 64 mL h^{-1} g^{-1}, respectively. To elucidate the contribution of delamination and framework type to these differences in the catalytic activities of the delaminated-zeolite catalysts, we compared these values to the nondelaminated three-dimensional zeolite catalysts Ti-SSZ-70 and Ti-ERB-1. Both of these catalysts show lower mass-based rate constants k of 29 mL (h g cat)$^{-1}$ and 21 mL (h g cat)$^{-1}$, for Ti-SSZ-70 and Ti-ERB-1, respectively. These rate constants are 2- to 3-fold lower than those of their delaminated counterparts (*i.e.* when correspondingly comparing Ti-SSZ-70 to Ti-DZ-2 and Ti-UCB-4 and Ti-ERB-1 to Ti-DZ-3). This is commensurate with the 2- to 3-fold lower Ti concentrations in nondelaminated zeotypes compared to their delaminated counterparts, a result of the lower external surface area of nondelaminated zeotypes onto which Ti can graft. The higher external surface area of delaminated zeotypes leads to more active catalysts by enabling a higher per-mass density of grafted sites on the surface.

The difference of the catalytic rate constants for the nondelaminated zeolites Ti-SSZ-70 and Ti-ERB-1 of 29 mL h^{-1} g^{-1} and 21 mL h^{-1} g^{-1} can be attributed to the higher external surface area of Ti-SSZ-70 (79 m^2 g^{-1}) compared to ERB-1 (50 m^2 g^{-1}) and the resulting higher Ti-content (see data in Table 3). However, when comparing the epoxidation rate constants k for the delaminated materials Ti-DZ-2 (k = 94 mL h^{-1} g^{-1}) and Ti-DZ-3 (k = 64 mL h^{-1} g^{-1}), which both possess comparable external surface areas of 110 m^2 g^{-1} and 94 m^2 g^{-1}, respectively, it is apparent that the difference in surface area alone cannot explain the difference in rate constant, as Ti-DZ-2 possesses 17% more external surface are but exhibits a 47% higher rate constant. These are trends reflected in the higher Ti-based rate constant for DZ-2 in Table 3. We hypothesize that both framework type (SSZ-70 for DZ-2 *vs.* MWW for DZ-3) and Ti-active site distribution within the framework has significant repercussions on catalytic performance. Separately, Ti-DZ-2 (k = 94 mL h^{-1} g^{-1}) and Ti-UCB-4 (k = 72 mL h^{-1} g^{-1}), both prepared from the same SSZ-70 precursor, have different catalytic activities at similar Ti loadings, suggesting that framework-type and active site distribution alone do not account for the observed differences in the delaminated-zeolite catalysts (*i.e.*, the same SSZ-70 framework leads to a catalyst of substantially different activity). We conclude that the combination of delamination synthetic approach coupled with the framework type is important for catalytic performance.

Overall, Ti-DZ-2 promises to be a highly active and stable catalyst for olefin epoxidation under harsh deactivating conditions, which are present under tail-end conditions of the flow reactor.

Conclusions

A synthetic approach enabling the delamination of BSSZ-70(P) – a layered zeolite precursor synthesized using a cationic quaternary ammonium structure directing agent – is demonstrated. This approach does not require long-chain surfactants and sonication and is therefore more practical and economic than current delamination methods. The approach is generalizable to other layered zeolite precursor frameworks, demonstrated by the delamination of ERB-1 with MWW framework topology, and may find particular utility in delaminated syntheses like SSZ-70 that require a quaternary ammonium structure directing agent, since prior delamination approaches that obviate sonication failed for this latter class of materials.

Successful delamination and preservation of intralayer integrity was verified by comparing physicochemical properties to those of the three-dimensional B-SSZ-70 and ERB-1 and, in the case of DZ-2, to those of UCB-4, a conventional delaminated variant of B-SSZ-70 that requires surfactant swelling and sonication for its synthesis. All materials were post-synthetically functionalized with Ti heteroatoms to introduce catalytic sites, which were characterized by UV-VIS spectroscopy. The Lewis acid-site character of both Ti-DZ-2 and Ti-DZ-3 was demonstrated by their ability to catalyze 1-octene epoxidation with EBHP, under harsh tail-end flow conditions. For SSZ-70-

topology, the new delaminated-zeolite catalyst Ti-DZ-2 exhibited the highest per-Ti-site activity, relative to all other materials including MWW-based zeolites Ti-DZ-3 and nondelaminated Ti-ERB-1. The similar selectivity of all delaminated zeolites relative to their nondelaminated counterparts is consistent with an intact crystalline framework surrounding the grafted Ti site, as characterized for DZ-2 *via* ^{29}Si MAS NMR and ^{29}Si CP/MAS NMR spectroscopies.

Conflicts of interest

The authors declare the following competing financial interests: (1) The funding for the research partially came from Chevron Energy Technology Co. and (2) X. O. and S. I. Z. are employees and stockholders in Chevron Corp. (3) A.K. and A.O. have ownership in Berkeley Materials Solutions, a company that is commercializing zeolitic materials for applications in catalysis, including olefin epoxidation.

Acknowledgements

The authors are grateful to the National Science Foundation (PFI: AIR-TT 1542974), which provided funding for enabling reported materials synthesis activities, and the Office of Basic Energy Sciences of U.S. Department of Energy (DE-FG02-05ER15696), which provided funding for undertaking all reported catalysis experiments. The authors are also grateful for the Management and Transfer of Hydrogen *via* Catalysis Program funded by Chevron Corporation, which provided funding for a postdoctoral fellowship to X. O. Work at the Molecular Foundry was supported by the Office of Science, Office of Basic Energy Sciences, of the U.S. Department of Energy under Contract No. DE-AC02-05CH11231. C. S. acknowledges Deutsche Forschungsgemeinschaft (DFG) for a research fellowship.

Notes and references

1 M. E. Davis, *Chem. – Eur. J.*, 1997, **3**, 1745–1750.
2 J. Jiang, J. Yu and A. Corma, *Angew. Chem., Int. Ed.*, 2010, **49**, 3120–3145.
3 A. Corma, V. Fornes, S. B. Pergher, T. L. M. Maesen and J. G. Buglass, *Nature*, 1998, **396**, 353–356.
4 S. Maheshwari, E. Jordan, S. Kumar, F. S. Bates, R. L. Penn, D. F. Shantz and M. Tsapatsis, *J. Am. Chem. Soc.*, 2008, **130**, 1507–1516.
5 W. J. Roth and J. Čejka, *Catal. Sci. Technol.*, 2011, **1**, 43.
6 N. D. Hould, S. Kumar, M. Tsapatsis, V. Nikolakis and R. F. Lobo, *Langmuir*, 2010, **26**, 1260–1270.
7 C. Anand, Y. Yamaguchi, Z. Liu, S. Ibe, S. P. Elangovan, T. Ishii, T. Ishikawa, A. Endo, T. Okubo and T. Wakihara, *Sci. Rep.*, 2016, **6**, 29210.
8 H. Y. Luo, V. K. Michaelis, S. Hodges, R. G. Griffin and Y. Román-Leshkov, *Chem. Sci.*, 2015, **6**, 6320–6324.
9 U. Díaz and A. Corma, *Dalton Trans.*, 2014, **43**, 10292–10316.
10 R. Schenkel, J. O. Barth, J. Kornatowski and J. A. Lercher, *Stud. Surf. Sci. Catal.*, 2002, **142**, 69–76.
11 I. Ogino, M. M. Nigra, S. J. Hwang, J. M. Ha, T. Rea, S. I. Zones and A. Katz, *J. Am. Chem. Soc.*, 2011, **133**, 3288–3291.
12 S. Maheshwari, C. Martínez, M. Teresa Portilla, F. J. Llopis, A. Corma and M. Tsapatsis, *J. Catal.*, 2010, **272**, 298–308.
13 X. Ouyang, Y.-J. Wanglee, S.-J. Hwang, D. Xie, T. Rea, S. I. Zones and A. Katz, *Dalton Trans.*, 2014, **43**, 10417–10429.
14 X. Ouyang, S. J. Hwang, R. C. Runnebaum, D. Xie, Y. J. Wanglee, T. Rea, S. I. Zones and A. Katz, *J. Am. Chem. Soc.*, 2014, **136**, 1449–1461.
15 S. Smeets, Z. J. Berkson, D. Xie, S. I. Zones, W. Wan, X. Zou, M. F. Hsieh, B. F. Chmelka, L. B. McCusker and C. Baerlocher, *J. Am. Chem. Soc.*, 2017, **139**, 16803–16812.
16 R. C. Runnebaum, X. Ouyang, J. a. Edsinga, T. Rea, I. Arslan, S. Hwang, S. I. Zones and A. Katz, *ACS Catal.*, 2014, **4**, 2364–2368.
17 X. Ouyang, S. J. Hwang, D. Xie, T. Rea, S. I. Zones and A. Katz, *ACS Catal.*, 2015, **5**, 3108–3119.
18 N. A. Grosso-Giordano, C. Schroeder, A. Okrut, A. Solovyov, C. Schöttle, W. Chassé, N. Marinković, H. Koller, S. I. Zones and A. Katz, *J. Am. Chem. Soc.*, 2018, **140**, 4956–4960.
19 M. Aigner, N. A. Grosso-Giordano, A. Okrut, S. Zones and A. Katz, *React. Chem. Eng.*, 2017, **2**, 842–851.
20 M. Aigner, N. A. Grosso-Giordano, C. Schöttle, A. Okrut, S. Zones and A. Katz, *React. Chem. Eng.*, 2017, **2**, 852–861.
21 W. J. Roth, P. Nachtigall, R. E. Morris and C. Jir, *Chem. Rev.*, 2014, **114**, 4807–4837.
22 A. Korzeniowska, J. Grzybek, W. J. Roth, A. Kowalczyk, P. Michorczyk, J. Čejka, J. Přech and B. Gil, *ChemCatChem*, 2018, 1–9.
23 J. Přech, P. Pizarro, D. P. Serrano and J. Čejka, *Chem. Soc. Rev.*, 2018, DOI: 10.1039/C8CS00370J, Advance Article.
24 J. Přech, *Catal. Rev. - Sci. Eng.*, 2018, **60**, 71–131.
25 M. V. Opanasenko, W. J. Roth and J. Čejka, *Catal. Sci. Technol.*, 2016, **6**, 2467–2484.
26 N. Tsunoji, M. V. Opanasenko, M. Kubů, J. Čejka, H. Nishida, S. Hayakawa, Y. Ide, M. Sadakane and T. Sano, *ChemCatChem*, 2018, **10**, 2536–2540.
27 M. Witman, S. Ling, P. Boyd, S. Barthel, M. Haranczyk, B. Slater and B. Smit, *ACS Cent. Sci.*, 2018, **4**, 235–245.
28 I. Ogino, E. A. Eilertsen, S. J. Hwang, T. Rea, D. Xie, X. Ouyang, S. I. Zones and A. Katz, *Chem. Mater.*, 2013, **25**, 1502–1509.
29 E. A. Eilertsen, I. Ogino, S. J. Hwang, T. Rea, S. Yeh, S. I. Zones and A. Katz, *Chem. Mater.*, 2011, **23**, 5404–5408.
30 G. E. Maciel and D. W. Sindorf, *J. Am. Chem. Soc.*, 1980, **102**, 7606–7607.
31 N. A. Grosso-Giordano, A. J. Yeh, A. Okrut, D. J. Xiao, F. Grandjean, G. J. Long, S. I. Zones and A. Katz, *Chem. Mater.*, 2017, **29**, 6480–6492.
32 P. Ratnasamy, D. Srinivas and H. Knözinger, *Adv. Catal.*, 2004, **48**, 1–169.

